

Heralded quantum entangling gate for distributed quantum computation in a decoherence-free subspace

Wanhua Su¹, Wei Qin², Adam Miranowicz^{2,3}, Tao Li^{1,4*}, and Franco Nori^{2,5,6}

¹MIT Key Laboratory of Semiconductor Microstructure and Quantum Sensing,

School of Science, Nanjing University of Science and Technology, Nanjing 210094, China

²Theoretical Quantum Physics Laboratory, Cluster for Pioneering Research, RIKEN, Wakoshi, Saitama 351-0198, Japan

³Institute of Spintronics and Quantum Information, Faculty of Physics,

Adam Mickiewicz University, PL-61-614 Poznań, Poland

⁴National Laboratory of Solid State Microstructures, Nanjing University, Nanjing 210093, China

⁵Quantum Computing Center, RIKEN, Wakoshi, Saitama 351-0198, Japan

⁶Physics Department, The University of Michigan, Ann Arbor, Michigan 48109-1040, USA

(Dated: May 2, 2023)

We propose a heralded nonlocal protocol for implementing an entangling gate on two stationary qubits coupled to spatially separated cavities. By dynamically controlling the evolution of the composite system, the entangling gate can be achieved without real excitations of cavity modes nor atoms. The success of our protocol is conditioned on projecting an auxiliary atom onto a postselected state, which simultaneously removes various detrimental effects of dissipation on the gate fidelity. In principle, the success probability of the gate can approach unity as the single-atom cooperativity becomes sufficiently large. Furthermore, we show its application for implementing single- and two-qubit gates within a decoherence-free subspace that is immune to a collective dephasing noise. This heralded, faithful, and nonlocal entangling gate protocol can, therefore, be useful for distributed quantum computation and scalable quantum networks.

I. INTRODUCTION

Quantum computation exploiting quantum systems for information processing has attracted a great deal of attention [1–5] due to its promising advantages over classical computation [6–8], and has been experimentally demonstrated with its superiority in handling well-defined tasks. These include implementing algorithms based on quantum gates [9, 10] and quantum annealing [11] using superconducting quantum processors, and performing boson sampling using linear-optical interferometers [12–14]. Nontrivial entangling quantum gates in combination with general single-qubit rotations in principle enable implementing various quantum algorithms for practical applications. The entangling quantum gates always involve direct or indirect interactions between the systems which they are applied on. So far, entangling quantum gates have been proposed for different physical systems, such as photons [15–20], trapped ions [21, 22], color centers [23–28], quantum dots [29–32], and superconducting circuits [33–36]. However, the scalability of quantum computation is challenging due to the inevitable presence of noise and decoherence. Fortunately, their influences on the evolution of quantum systems can be suppressed by the use of e.g.: dynamical decoupling [37, 38], holonomic manipulation [39–41], and decoherence-free subspaces (DFSs) [42–45]. Moreover, a certain amount of noise and decoherence can be tolerated by harnessing quantum error correction codes [46], in which the

overheads and the complexity considerably increase with the error rate.

For some specific dominant noise or decoherence [42], DFSs can provide an efficient method for protecting the logical qubits against noise by encoding quantum information in a DFS [47–51]. A fundamental and dominant noise in stationary systems is dephasing due to the random fluctuations of external fields [50], which destroy the coherence between two computational basis states. A simple DFS for tackling this issue can be constructed by properly encoding a logical qubit with two physical qubits, which simultaneously suffers from the same phase noise (i.e., collective dephasing noise) [42]. Exploiting DFS for quantum computation has been widely studied using various platforms [52–65]. For these protocols, a DFS can work in a deterministic way by dynamically controlling the evolution of systems, or in a heralded way with the detection of single photons scattered by cavity-coupled platforms. Furthermore, some significant experimental efforts have been made for the realization of quantum gates acting on decoherence-free systems [66–69].

Recently, a heralded method for achieving effective quantum computation [70–72] has been presented by dynamically controlling the evolution rather than by scattering and measuring single photons. Borregaard *et al.* [70] proposed a heralded, near-deterministic protocol for performing quantum gates on natural atoms trapped in a single optical cavity. Qin *et al.* [71] presented heralded, nonlocal-controlled entangling gates on superconducting qubits coupled to the same cavity, and introduced a second cavity coupled to an auxiliary qubit for a heralding operation. These protocols provide a *quadratic fidelity improvement* compared to previous

*tao.li@njust.edu.cn

deterministic cavity-based gates, and can find their applications in long-distance entanglement distribution and quantum computation [72–75]. However, it is noteworthy that nonlocal entangling gates for stationary qubits coupled to different optical cavities are useful for distributed quantum computation [76–79] and for realizing quantum repeater networks [80–86]. Hence it is important to generalize the heralded schemes of Refs. [70, 71] to the *nonlocal* case.

In this paper, we propose a heralded method for implementing entangling quantum gates of *nonlocal* stationary qubits coupled to different cavities by dynamically controlling the evolution of cavity-coupled systems. The cavities can be connected by short fibers or superconducting coaxial cables [87]. A four-level auxiliary atom is coupled to an additional cavity as both a virtual-photon source and a detector for heralding the success of the quantum gate [70, 71]. According to the results of a proper measurement on the auxiliary atom, *the gate errors introduced by atomic spontaneous emission and cavity photon loss can be inherently removed, leading to faithful nonlocal entangling gates*. As a result, the detected errors simply lower the success probability of the gate rather than its fidelity, which is extremely important for practical applications [76–86].

We show that *the fidelity of our two-qubit nonlocal entangling gate can be further improved by applying proper single-qubit operations to the qubits after the entangling gate*. Furthermore, we propose an approach for performing a heralded quantum entangling gate in a DFS. Each logical qubit consisting of two physical qubits couples to an individual cavity and suffers from different dephasing noises. Combining the advantages of heralded inherent error detection and error-avoiding DFS, our nonlocal entangling gate can directly find its applications in distributed quantum computation and quantum networks.

The remaining of the paper is organized as follows: In Sec. II, we describe a prototype physical model for the heralded nonlocal entangling gate on two spatially separated qubits. In Sec. III, we give an effective master equation to simulate the quantum dynamics. In Sec. IV, we describe an implementation of a heralded nonlocal CPHASE gate and analyze its performance. In Sec. V, we present heralded nonlocal entangling gates operating on logical qubits in a DFS immune to collective dephasing noise. Finally, we conclude with a brief discussion and summary in Sec. VI.

II. PROTOTYPE PHYSICAL MODEL FOR A HERALDED ENTANGLING GATE

An essential building block for heralded nonlocal entangling gates is the use of cavity-coupled systems [87]. They can be implemented by various natural or artificial atoms [4] coupled to optical cavities (including

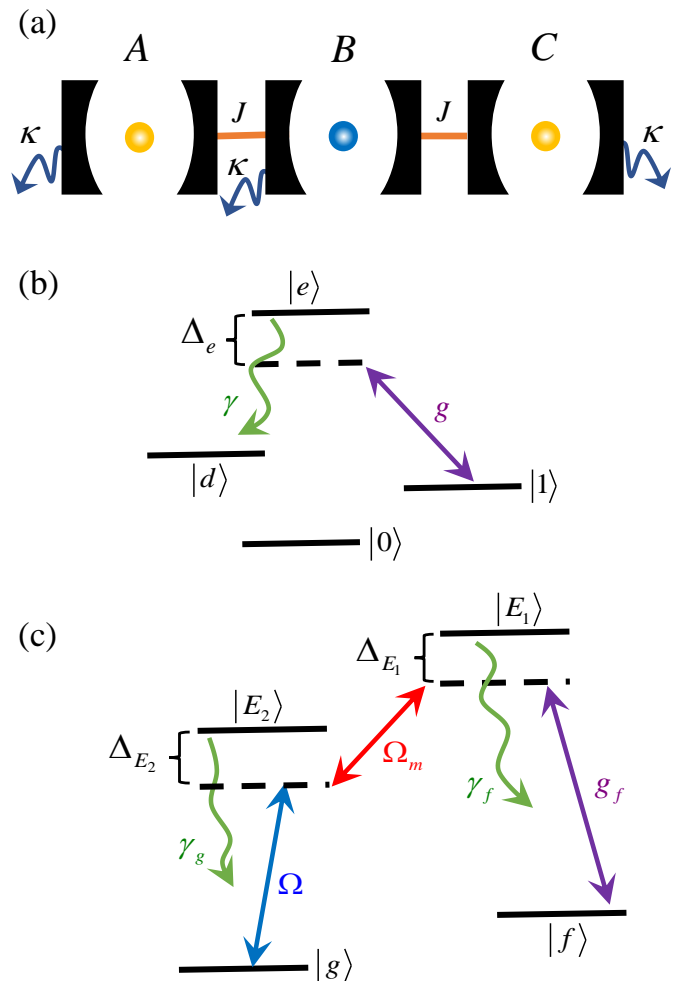


FIG. 1: Schematics of a heralded nonlocal entangling gate. (a) Implementation of the gate with a cavity-coupled system. Two stationary qubits are distributed in two separated cavities that are connected to an auxiliary cavity via short fibers or superconducting coaxial cables. (b) Level structure of two qubit-encoding atoms coupled to the cavities A and C. (c) Level structure of the auxiliary atom that couples to the cavity B and works as a heralding system.

transmission-line resonators), which can be connected by short optical fibers (or superconducting coaxial cables).

The schematics of our heralded nonlocal entangling gate protocol is shown in Fig. 1. Two qubit-encoding atoms couple to two separated cavities A and C that are connected via short optical fibers, and an auxiliary atom couples to the cavity B in the middle. The effective coupling between two neighboring cavities can be described by a coupling rate J when the fiber length L is small and two cavities are resonant [88, 89]. Each qubit-encoding atom has two ground levels ($|0\rangle$ and $|1\rangle$), which can encode a qubit, and one excited level $|e\rangle$, shown in Fig. 1(b).

We assume that the transition $|1\rangle \leftrightarrow |e\rangle$ of both qubit-encoding atoms is coupled to the cavity mode with a

coupling rate $g > 0$ and a detuning Δ_e , and that the excited level $|e\rangle$ decays to a level $|d\rangle$, which may or may not be $|0\rangle$ or $|1\rangle$.

The auxiliary atom has two ground states $|g\rangle$ and $|f\rangle$ and two excited states $|E_1\rangle$ and $|E_2\rangle$, shown in Fig. 1(c). The $|f\rangle \leftrightarrow |E_1\rangle$ transition couples to the cavity mode a_B with a coupling rate $g_f > 0$ and a detuning Δ_{E_1} . The transition between states $|E_2\rangle$ and $|E_1\rangle$ ($|g\rangle$ and $|E_2\rangle$) is driven by a classical field with frequency ω_m (ω_L) and Rabi frequency Ω_m (Ω). Therefore, a three-photon resonant transition, resulting in a flip of two ground states of the auxiliary atom, can be achieved by tuning the driving frequency Ω_m and Ω .

The states $|E_1\rangle$ and $|E_2\rangle$ spontaneously decay to the states $|f\rangle$ and $|g\rangle$ with rates γ_f and γ_g , respectively. Therefore, the total Hamiltonian of the composite system, consisting of the three atoms and three cavities, can be written as

$$H_T = H_0 + H_1, \quad (1)$$

where H_0 and H_1 represent the free and interaction Hamiltonians, respectively. The free Hamiltonian H_0 is detailed as

$$\begin{aligned} H_0 = & \sum_{k=1,2} (\omega_e |e\rangle_k \langle e| + \omega_1 |1\rangle_k \langle 1| + \omega_0 |0\rangle_k \langle 0|) \\ & + \omega_{E_1} |E_1\rangle \langle E_1| + \omega_{E_2} |E_2\rangle \langle E_2| + \omega_f |f\rangle \langle f| \\ & + \omega_g |g\rangle \langle g| + \omega_c (a_A^\dagger a_A + a_B^\dagger a_B + a_C^\dagger a_C), \quad (2) \end{aligned}$$

where ω_x is the frequency of the atomic level $|x\rangle$, except ω_c , which is the common resonance frequency of the three cavities. The interaction Hamiltonian H_1 (including the cavity-cavity coupling, the atom-cavity coupling, and the classical driving) becomes

$$\begin{aligned} H_1 = & \left[g(a_A |e\rangle_1 \langle 1| + a_C |e\rangle_2 \langle 1|) + g_f a_B |E_1\rangle \langle f| \right. \\ & + \frac{1}{2} (\Omega e^{-i\omega_L t} |E_2\rangle \langle g| + \Omega_m e^{-i\omega_m t} |E_1\rangle \langle E_2|) \\ & \left. + J(a_A a_B^\dagger + a_C a_B^\dagger) \right] + \text{H.c.}, \quad (3) \end{aligned}$$

where H.c. represents the Hermitian conjugate, and we have assumed a symmetry coupling between two qubit-encoding atoms and their corresponding cavities.

In order to explicitly describe the dynamics of the composite system, we perform a Bogoliubov transformation for the three cavity modes and introduce three delocalized bosonic modes as:

$$\begin{aligned} c_1 &= \frac{1}{2}(a_A - \sqrt{2}a_B + a_C), \\ c_2 &= \frac{1}{2}(a_A + \sqrt{2}a_B + a_C), \\ c_3 &= \frac{1}{\sqrt{2}}(a_A - a_C). \quad (4) \end{aligned}$$

The total Hamiltonian in the new basis can be described, in a proper rotating frame, as

$$H_T = H_e + V + V^\dagger, \quad (5)$$

where H_e and V describe the evolution of the single-excitation subspace and its coupling to the ground space, respectively. Specifically, they can be expressed as

$$\begin{aligned} H_e = & \Delta_{E_1} |E_1\rangle \langle E_1| + \Delta_{E_2} |E_2\rangle \langle E_2| \\ & + \left[\frac{\Omega_m}{2} |E_1\rangle \langle E_2| + \text{H.c.} \right] + H_{e1}, \quad (6) \end{aligned}$$

where

$$\begin{aligned} H_{e1} = & \sum_{k=1,2} \left[\frac{g}{2} (c_1 + c_2 + \sqrt{2}S_k c_3) |e\rangle_k \langle 1| + \text{H.c.} \right] \\ & + \Delta_e |e\rangle_k \langle e| + \left\{ \left[\frac{g_f}{\sqrt{2}} (c_2 - c_1) |E_1\rangle \langle f| + \text{H.c.} \right] \right. \\ & \left. + \sqrt{2}J(2c_2^\dagger c_2 + c_3^\dagger c_3) \right\}, \quad (7) \end{aligned}$$

with $S_k = (-1)^{k+1}$ and $V = \frac{\Omega}{2} |E_2\rangle \langle g|$. Here, for simplicity, we have defined some detunings as follows:

$$\begin{aligned} \Delta_{E_1} &= \omega_{E_1} - \omega_L - \omega_m - \omega_g, \\ \Delta_{E_2} &= \omega_{E_2} - \omega_L - \omega_g, \\ \Delta_e &= \omega_e - \omega_L - \omega_m + \omega_f - \omega_g - \omega_1. \quad (8) \end{aligned}$$

For large detunings (i.e., $\Delta_{E_1} \gg \Omega$ and $\Delta_{E_2} \gg \Omega_m$) and a large coupling strength (i.e., $J \gg g_f$) between two neighboring cavities, we can effectively eliminate the excited states $|E_1\rangle$ and $|E_2\rangle$ and then obtain a three-photon resonant Raman transition from $|g\rangle \rightarrow |f\rangle$, which is mediated by the mode c_1 rather than the modes $c_{2,3}$ if the driving field frequency is tuned to

$$\omega_L = \omega_c - \omega_m + \omega_f - \omega_g - \sqrt{2}J. \quad (9)$$

The evolution of the composite system consisting of two qubit-encoding atoms, a single auxiliary atom, and three cavities connected by optical fibers can in principle be identical to that of two qubit-encoding atoms and one auxiliary atom, all coupled to the same cavity.

By adiabatically eliminating the state $|E_2\rangle$ of the auxiliary atom and moving into a proper rotating frame, the effective Hamiltonian of the composite system can be described by $H'_T = H'_e + V' + V'^\dagger$, with an effective three-level auxiliary atom. Here,

$$\begin{aligned} H'_e = & \left(\Delta_{E_1} + \frac{\Omega^2 - \Omega_m^2}{4\Delta_{E_2}} \right) |E_1\rangle \langle E_1| \\ & + \left(\Delta_{E_2} + \frac{\Omega^2}{4\Delta_{E_2}} \right) |E_2\rangle \langle E_2| + H_{e1}, \quad (10) \end{aligned}$$

and

$$V' = -\tilde{\Omega} |E_1\rangle \langle g|, \quad \tilde{\Omega} = \frac{\Omega_m \Omega}{2\Delta_{E_2}}. \quad (11)$$

When all qubit-encoding atoms are in the state $|0\rangle$ that is decoupled from the mode c_1 , an adiabatic excitation of the auxiliary atom results in the dark zero-energy state:

$$|\psi\rangle_d = \frac{1}{\sqrt{g_f^2 + 2\tilde{\Omega}^2}} \left(g_f |0, 0, 0, g\rangle - \sqrt{2}\tilde{\Omega} |1, 0, 0, f\rangle \right), \quad (12)$$

where $|0, 0, 0, g\rangle$ represents that the three cavity modes are in the vacuum state and the auxiliary is in the state $|g\rangle$, while $|1, 0, 0, f\rangle$ represents that the mode c_1 has a single photon, the modes c_2 and c_3 are in the vacuum state, and the auxiliary atom is in the state $|f\rangle$.

In contrast, when either or both qubit atoms are in the state $|1\rangle$, they couple to the mode c_1 and introduce an ac Stark shift, which causes a dynamical phase after applying the driving. Therefore, all the qubit states except the uncoupled one acquire a phase that is determined by the duration of the driving field, which is essential for constructing various heralded entangling gates (as shown below).

III. EFFECTIVE MASTER EQUATION

So far, we have described our nonlocal heralded entangling gate protocol for an ideal case in which the composite system is decoupled from its environment. Here we use the master equation in the Lindblad form to study the dissipative dynamics of our system. We assume that the dissipation of the system is described by the Lindblad operators: $L_{c_l} = \sqrt{\kappa}c_l$ with $l = 1, 2, 3$ represents the photon loss of the cavity modes with the same dissipation rate κ ; $L_f = \sqrt{\gamma_f}|f\rangle\langle E_1|$ and $L_g = \sqrt{\gamma_g}|g\rangle\langle E_2|$ describe the decay of the auxiliary atom with rates γ_f and γ_g ; and $L_k = \sqrt{\gamma}|d\rangle\langle e|$ ($k = 1, 2$) describes the decay of the qubit-encoding atoms with rate γ . We assume that the excited level $|e\rangle$ decays to some level $|d\rangle$, which, in fact, may or may not be $|1\rangle$ or $|0\rangle$, since the decay of either a cavity or an excited atom leads to a heralded error.

The standard master equation in the Lindblad form for the composite system described by the Hamiltonian in Eq. (5) can be given by

$$\dot{\rho}_T(t) = i[\rho_T(t), H_T] + \frac{1}{2} \sum_j \left[2L_j \rho_T(t) L_j^\dagger - \rho_T(t) L_j^\dagger L_j - L_j^\dagger L_j \rho_T(t) \right], \quad (13)$$

where $\rho_T(t)$ represents the density matrix of the total system.

For a weak classical driving field, i.e., $\{\Omega/\Delta_{E_2}, \Omega/g\} \ll 1$, the excitations of the cavity modes and the excited states of the atoms can be adiabatically eliminated, when the system is initially prepared in the ground-state subspace. Therefore, the ground-state evolution of the composite system can be described by an effective master equation as follows [90, 91]:

$$\dot{\rho} = i[\rho, H_{\text{eff}}] + \frac{1}{2} \sum_j \left\{ 2L_{\text{eff}}^j \rho (L_{\text{eff}}^j)^\dagger - \left[(L_{\text{eff}}^j)^\dagger L_{\text{eff}}^j \rho + \rho (L_{\text{eff}}^j)^\dagger L_{\text{eff}}^j \right] \right\}. \quad (14)$$

Here ρ denotes the ground-space density matrix of the composite system; H_{eff} represents an effective Hamiltonian given by

$$H_{\text{eff}} = -\frac{1}{2} V^\dagger \left[H_{\text{NH}}^{-1} + (H_{\text{NH}}^{-1})^\dagger \right] V, \quad (15)$$

and L_{eff}^j are the effective Lindblad operators with

$$L_{\text{eff}}^j = L_j H_{\text{NH}}^{-1} V, \quad (16)$$

while the non-Hermitian Hamiltonian H_{NH} governing the dynamics of the decaying excited states [91] can be given, in the quantum jump formalism, as

$$\begin{aligned} H_{\text{NH}} &= H_e - \frac{i}{2} \sum_j L_j^\dagger L_j \\ &= \sum_{k=1,2} \left[\frac{\bar{\Delta}_e}{2} |e\rangle_k \langle e| + \frac{g}{2} (c_1 + c_2 + \sqrt{2} S_k c_3) |e\rangle_k \langle 1| \right. \\ &\quad \left. + \text{H.c.} \right] + \bar{\Delta}_{E_1} |E_1\rangle \langle E_1| + \bar{\Delta}_{E_2} |E_2\rangle \langle E_2| - \frac{i\kappa}{2} c_1^\dagger c_1 \\ &\quad + \sum_{l=2,3} \bar{J}_l c_l^\dagger c_l + \frac{gf}{\sqrt{2}} [(c_2 - c_1) |E_1\rangle \langle f| + \text{H.c.}] \\ &\quad + \frac{\Omega_m}{2} (|E_1\rangle \langle E_2| + \text{H.c.}), \end{aligned} \quad (17)$$

where $\bar{\Delta}_{E_1} = \Delta_{E_1} - i\gamma_f/2$, $\bar{\Delta}_{E_2} = \Delta_{E_2} - i\gamma_g/2$, $\bar{\Delta}_e = \Delta_e - i\gamma/2$, $\bar{J}_2 = 2\sqrt{2}J - i\kappa/2$, and $\bar{J}_3 = \sqrt{2}J - i\kappa/2$.

To achieve the nonlocal heralded gate, the composite system is confined within the zero- and single-excitation subspaces. The effective Hamiltonian H_{eff} and the effective Lindblad operators L_{eff}^j can be directly derived from Eqs. (15)–(17). Specifically, H_{eff} is given as follows:

$$H_{\text{eff}} = |g\rangle \langle g| \otimes \sum_{N=0}^2 \Delta_N \mathcal{P}_N, \quad (18)$$

where \mathcal{P}_N is a projection operator that projects the two qubit-encoding atoms onto a state with N qubits in $|1\rangle$, while Δ_N represents the N -dependent ac Stark shift which can be expressed as

$$\begin{aligned} \Delta_N &= -\frac{\Omega^2}{\gamma} \text{Re} \left\{ \frac{1}{\mathcal{X}_N} \left[C \tilde{\Delta}_e (m+n) (S_1 + \tilde{J}_2 S_2) \right. \right. \\ &\quad \left. \left. - 2\tilde{\Delta}_e^2 \tilde{J}_2 S_1 - 2mnC^2 S_2 \right] \right\}, \end{aligned} \quad (19)$$

where Re denotes the real part of an argument, $m(n) \in \{0, 1\}$ denotes the number of the qubit-encoding atoms in the state $|1\rangle$, and coupled to cavity A (C). Moreover, $C = g^2/(\gamma\kappa)$, $C_f = g_f^2/(\gamma\kappa)$, $\tilde{\Delta}_{E_1} = \Delta_{E_1}/\gamma - i\gamma_f/(2\gamma)$, $\tilde{\Delta}_{E_2} = \Delta_{E_2}/\gamma - i\gamma_g/(2\gamma)$, $\tilde{\Delta}_e = \Delta_e/\gamma - i/2$, $\tilde{J}_1 = 2\sqrt{2}J/\kappa - i/2$, $\tilde{J}_2 = \sqrt{2}J/\kappa - i/2$, $\tilde{\Omega}_m = \Omega_m/\gamma$, $Z = 4\tilde{\Delta}_{E_1}\tilde{\Delta}_{E_2} - \tilde{\Omega}_m^2$, $S_1 = C_f (2i\tilde{J}_1 + 1) - 2\tilde{\Delta}_{E_1}\tilde{J}_1$, $S_2 = 4iC_f - \tilde{\Delta}_{E_1}(2i\tilde{J}_1 + 1)$, and $\mathcal{X}_N = C_f \tilde{\Delta}_{E_2} R_2 - R_1 Z$ with

$$R_1 = \tilde{\Delta}_e C (m+n) (\tilde{J}_2 + 2\tilde{J}_1 + 2i\tilde{J}_1\tilde{J}_2)$$

$$-2C^2mn(2i\tilde{J}_1+1)-4\tilde{\Delta}_e^2\tilde{J}_1\tilde{J}_2 \quad (20)$$

and

$$R_2=4\tilde{\Delta}_eC(m+n)\left[2i(\tilde{J}_1+2\tilde{J}_2)+1\right]-32iC^2mn-8\tilde{\Delta}_e^2\tilde{J}_2(2i\tilde{J}_1+1). \quad (21)$$

The effective Lindblad operators are expressed as follows:

$$\begin{aligned} L_{\text{eff}}^g &= |g\rangle\langle g| \otimes \sum_{N=0}^2 r_{g,N}\mathcal{P}_N, \\ L_{\text{eff}}^f &= |f\rangle\langle g| \otimes \sum_{N=0}^2 r_{f,N}\mathcal{P}_N, \\ L_{\text{eff}}^{c_1} &= |f\rangle\langle g| \otimes \sum_{N=0}^2 r_{c_1,N}\mathcal{P}_N, \\ L_{\text{eff}}^k &= |f\rangle\langle g| \otimes \sum_{N=1}^2 r_{k,N}|d\rangle_k\langle 1|\mathcal{P}_N, \end{aligned} \quad (22)$$

where $k = 1$ ($k = 2$) labels the qubit-encoding atom coupled to cavity A (C) in the state $|1\rangle$. The corresponding effective decay rates $r_{g,N}$, $r_{f,N}$, $r_{c_1,N}$, and $r_{k,N}$ are given by:

$$\begin{aligned} r_{g,N} &= \frac{2\Omega\sqrt{\gamma_g}}{\gamma\mathcal{X}_N} \left[C\tilde{\Delta}_e(m+n)(S_1+\tilde{J}_2S_2) - 2\tilde{\Delta}_e^2\tilde{J}_2S_1 - 2mnC^2S_2 \right], \\ r_{f,N} &= \frac{\Omega\tilde{\Omega}_mR_1\sqrt{\gamma_f}}{\gamma\mathcal{X}_N}, \\ r_{c_1,N} &= 2\sqrt{2}i\delta \left[\tilde{\Delta}_eC(\tilde{J}_1+\tilde{J}_2)(m+n) - 2\tilde{\Delta}_e^2\tilde{J}_1\tilde{J}_2 - 2C^2mn \right], \\ r_{c_2,N} &= \sqrt{2}\delta \left[2\tilde{\Delta}_e^2\tilde{J}_2 + 4iC^2mn - C\tilde{\Delta}_e(1+2i\tilde{J}_2)(m+n) \right], \\ r_{c_3,N} &= C\delta \left[\tilde{\Delta}_e(1-2i\tilde{J}_1)(m-n) \right], \\ r_{1,N} &= r(n), \\ r_{2,N} &= r(m), \end{aligned} \quad (23)$$

where $r(k) = \sqrt{2C}\delta[(1-2i\tilde{J}_1)(kC-\tilde{\Delta}_e\tilde{J}_2)]$ and $\delta = \sqrt{C_f}\Omega\tilde{\Omega}_m/(\sqrt{\gamma}\mathcal{X}_N)$.

For a weak field, driving the transition $|E_1\rangle \rightarrow |E_2\rangle$ with $\Omega_m/\Delta_{E_2} \ll 1$, the ac Stark shift Δ_N and the effective decay rates $r_{i,N}$, shown in Eqs. (19) and (23), can be simplified:

$$\begin{aligned} \Delta_N &= -\frac{\Omega^2}{4\Delta_{E_2}} - \frac{\tilde{\Omega}^2}{4\gamma} \text{Re}\left(\frac{Q}{\mathcal{Y}_N}\right), \\ r_{f,N} &= -\frac{\tilde{\Omega}Q\sqrt{\gamma_f}}{2\gamma\mathcal{Y}_N}, \end{aligned}$$

$$\begin{aligned} r_{g,N} &= \frac{\Omega\sqrt{\gamma_g}}{2\Delta_{E_2}} + \frac{\tilde{\Omega}Q\sqrt{\gamma_g}}{2\gamma\mathcal{Y}_N}, \\ r_{c_1,N} &= 2\sqrt{2}\delta' \left[2\tilde{\Delta}_e^2\tilde{J}_1\tilde{J}_2 + 2C^2mn - C\tilde{\Delta}_e(\tilde{J}_1+\tilde{J}_2)(m+n) \right], \\ r_{c_2,N} &= \sqrt{2}\delta' \left[2i\tilde{\Delta}_e^2\tilde{J}_2 - 4C^2mn + C\tilde{\Delta}_e(2\tilde{J}_2-i)(m+n) \right], \\ r_{c_3,N} &= \delta' \left[C\tilde{\Delta}_e(i+2\tilde{J}_1)(m-n) \right], \\ r_{1,N} &= \alpha'r(n), \\ r_{2,N} &= \alpha'r(m), \end{aligned} \quad (24)$$

where $\delta' = \tilde{\Omega}\sqrt{C_f}/(2\mathcal{Y}_N\sqrt{\gamma})$, $\alpha' = i\tilde{\Omega}\mathcal{X}_N/(2\Omega\Omega_m\mathcal{Y}_N)$, and $\mathcal{Y}_N = C_fR + \tilde{\Delta}_{E_1}Q$, with:

$$\begin{aligned} R &= 2\tilde{\Delta}_e^2(-i+2\tilde{J}_1)\tilde{J}_2 + 8C^2mn - C\tilde{\Delta}_e(-i+2\tilde{J}_1+4\tilde{J}_2)(m+n), \\ Q &= 4i\tilde{\Delta}_e\tilde{J}_1\tilde{J}_2 + 2C^2(i-2\tilde{J}_1)mn + C\tilde{\Delta}_e[2\tilde{J}_1\tilde{J}_2 - i(\tilde{J}_2+2\tilde{J}_1)](m+n). \end{aligned} \quad (25)$$

We note that $\tilde{\Omega} = \Omega\Omega_m/(2\Delta_{E_2})$ is the effective Rabi frequency of the transition $|g\rangle \rightarrow |E_1\rangle$ and $\tilde{\gamma}_g = \gamma_g\Omega_m^2/(2\Delta_{E_2})^2$ is an effective decay rate of the excited state $|E_1\rangle$ to $|g\rangle$.

In practice, the auxiliary and the qubit-encoding atoms can be different. Their atom-cavity cooperativities and decay rates can be parameterized by $C_f = \alpha C$ and $\gamma_f = \beta\gamma$. For simplicity, we set $\alpha = \beta = 1$ in all our numerical simulations to show the influence of the cooperativity C on the system evolution. In this case, Δ_N and $r_{g,N}$ can be further simplified as:

$$\begin{aligned} \Delta_N &= -\frac{\tilde{\Omega}^2}{4\gamma} \text{Re}\left(\frac{Q}{\mathcal{Y}_N}\right), \\ r_{g,N} &= \frac{\Omega\sqrt{\gamma_g}}{2\Delta_{E_2}}, \end{aligned} \quad (27)$$

where the first term, $-\Omega^2/(4\Delta_{E_2})$, of Δ_N in Eq. (24) has been removed, because it is independent of the state of the qubits and, thus, has no influence on the phase gates. Furthermore, the second term of $r_{g,N}$ has also been removed for $\tilde{\gamma}_g \ll 1$, because the decay of the auxiliary-atom excited state to $|g\rangle$ is suppressed by a large detuning Δ_{E_2} .

Each Lindblad operator shown in Eq. (22), except L_{eff}^g (i.e., the dephasing of $|g\rangle$), represents various effective dissipative processes, leading to the transition $|g\rangle \rightarrow |f\rangle$. These are the dominant error factors that drive the system out of its effective subspace. Fortunately, the errors introduced by these dissipative processes can be inherently detected, because the success of each nonlocal

entangling gate is heralded by the measurement result $|g\rangle$ of the auxiliary atom. For heralded gates, these detectable decays have no effect on the fidelity, but decrease their success probability.

The success probability P of detecting the auxiliary atom in the state $|g\rangle$ can be obtained by solving the effective Lindblad master equation, given in Eq. (14), with the following definition

$$P = \sum_{N=0}^2 \text{Tr} [(|g\rangle \langle g| \otimes \mathcal{P}_N) \rho(t)], \quad (28)$$

where Tr is the trace operation over the subspace spanned by the ground states of the auxiliary and qubit-encoding atoms.

After the measurement on the auxiliary atom, the conditional density operator of the two qubit-encoding atoms is reduced to

$$\begin{aligned} \rho_{\text{qubit}}(t) = & \frac{1}{P} \sum_{N, N'=0}^2 e^{-i(\Delta_N - \Delta_{N'})t} e^{-(\Gamma_N + \Gamma_{N'})t/2} \\ & \times \mathcal{P}_N [\langle g| \rho(0) |g\rangle] \mathcal{P}_{N'}. \end{aligned} \quad (29)$$

Here the total decay rate Γ_N for N qubit-encoding atoms in the state $|1\rangle$ is found to be

$$\Gamma_N = |r_{f,N}|^2 + \sum_{l=1}^3 |r_{cl,N}|^2 + m|r_{1,N}|^2 + n|r_{2,N}|^2, \quad (30)$$

where $r_{g,N}$, $r_{f,N}$, $r_{cl,N}$, and $r_{k,N}$ are the effective decay rates given in Eq. (23). By properly controlling the evolution time and measuring the auxiliary atom, we can in principle achieve a two-qubit nonlocal controlled-phase (CPHASE) gate in a heralded way, as described below. The success probability of the gate is equal to that of projecting the auxiliary atom onto state $|g\rangle$.

IV. HERALDED NONLOCAL CPHASE GATE AND ITS PERFORMANCE

The effective Hamiltonian in Eq. (18) shows that the energy shift depends on the number of qubit-encoding atoms in state $|1\rangle$ when the auxiliary atom is in the state $|g\rangle$. Therefore, the time evolution under this effective Hamiltonian gives rise to different dynamical phases for the two qubits in the states $|00\rangle$, $|10\rangle$, $|01\rangle$, and $|11\rangle$. By choosing a suitable evolution time and then performing single-qubit transformations, we can achieve a phase flip of the qubit state $|11\rangle$, while leaving the other three states unchanged, which achieves the heralded nonlocal CPHASE gate on the two nonlocal atom qubits.

The detrimental effect of dissipative processes on the CPHASE gate, represented by the state flip of the auxiliary atom, can be inherently removed by projecting the auxiliary atom onto the state $|g\rangle$, while the state-dependent decay rate Γ_N of the qubit-encoding atoms

and the finite spontaneous decay rate $\tilde{\gamma}_g > 0$ can introduce extra errors. Therefore, we can improve the gate fidelity by modifying the system to achieve a state-independent decay rate, i.e., $\Gamma_0 = \Gamma_1 = \Gamma_2$. The state-independent total decay rate Γ_N , in the limit $\{G, C\} \gg 1$, where $G = J/\kappa$, can be given by

$$\Gamma_N = \Gamma = \frac{\tilde{\Omega}^2}{2\gamma} \frac{1}{\alpha C}, \quad (31)$$

where the detunings are changed to

$$\begin{aligned} \frac{\Delta_{E_1}}{\gamma} &= \alpha CD / \sqrt{2}, \\ \frac{\Delta_e}{\gamma} &= \frac{-2 + C(\bar{G}^2 - 4D\bar{G})}{2\sqrt{2}(\bar{G} - 2D)}, \end{aligned} \quad (32)$$

where $\bar{G} = 1/G$ and $D = \sqrt{\beta/\alpha C}$ are two auxiliary parameters. The corresponding energy shift can be rewritten as:

$$\begin{aligned} \Delta_0 &= -\Gamma \frac{(4D - \bar{G})}{8\sqrt{2}}, \\ \Delta_1 &= -\frac{\Gamma}{\sqrt{2}} \frac{2D - \bar{G}}{2/C + \bar{G}^2 - D\bar{G} + 2D^2}, \\ \Delta_2 &= -\frac{\Gamma}{\sqrt{2}} \frac{2D - \bar{G}}{1/C + \bar{G}^2/2 - D\bar{G} + 2D^2}, \end{aligned} \quad (33)$$

where Δ_0 approaches zero for $\{G, C\} \gg 1$, while Δ_1 and Δ_2 are nonzero and approximately equal to each other. This property can be used to achieve a heralded nonlocal CPHASE gate by a driving pulse with duration $T_\pi = \pi/|\Delta_2|$.

In practice, we can further decrease the gate error to arbitrarily small by performing unitary single-qubit rotations on each qubit-encoding atom, which depends on the dynamical evolution of the composite system. The duration of the driving pulse length is chosen to be

$$t_{\text{CZ}} = \frac{\pi}{|\Delta_2 - 2\Delta_1 + \Delta_0|}, \quad (34)$$

and the single-qubit rotation on each qubit after applying the pulse reads:

$$\begin{aligned} \mathcal{U}|0\rangle &= \exp(i\Delta_0 t_{\text{CZ}}/2) |0\rangle, \\ \mathcal{U}|1\rangle &= \exp[i(2\Delta_1 - \Delta_0) t_{\text{CZ}}/2] |1\rangle. \end{aligned} \quad (35)$$

These processes result in a phase flip of the state $|11\rangle$, while leaving the other three states (i.e., $|00\rangle$, $|10\rangle$, and $|01\rangle$) unchanged.

The success probability of the heralded nonlocal entangling gate equals that of finding the auxiliary atom in the state $|g\rangle$ at the end of the gate operation, and can be given by

$$P_{\text{CZ}} = \exp(-\Gamma t_{\text{CZ}}). \quad (36)$$

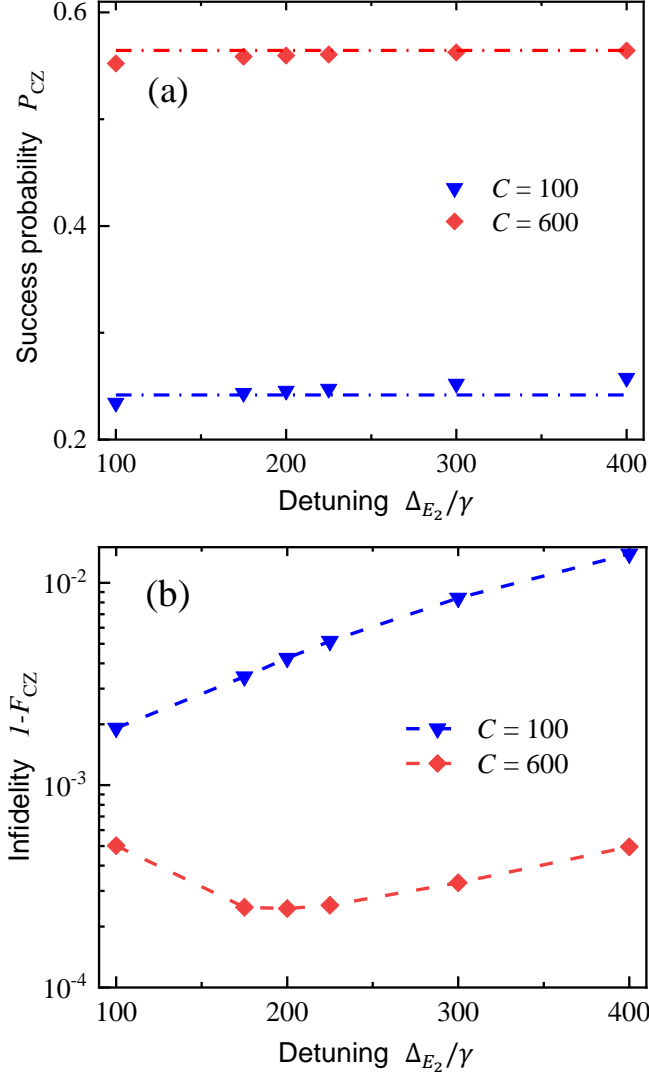


FIG. 2: Numerical simulations for the success probability and infidelity of the heralded nonlocal CPHASE gate with two cooperativities $C = 100$ (blue down-triangles) and $C = 600$ (red diamonds). (a) The success probability, P_{CZ} , of the gate as a function of the detuning Δ_{E_2} . Simultaneously, we also plot the analytical success probability (curves), which is in good agreement with the numerical values. (b) Infidelity, $1 - F_{CZ}$, of the CPHASE gate versus the detuning Δ_{E_2} . In both panels, we have set: $\lambda = 10$, $\gamma_g = \gamma_f = \gamma = 0.1\kappa$, $g = g_f$, $C = g^2/(\kappa\gamma)$, $\lambda = J/(\kappa\sqrt{C})$, $\alpha = \beta = 1$, $\Omega = \Delta_{E_2}/(6C^{1/4})$, and $\Omega_m = 4\gamma C^{1/4}$.

It can be further approximated as

$$P_{CZ} = 1 - Z_p \frac{\pi}{\sqrt{C}}, \quad (37)$$

for $\{C, G\} \gg 1$, where the scaling factor Z_p , with $\lambda = G/\sqrt{C}$ and $d = \sqrt{\beta/\alpha}$, can be given as

$$Z_p = \sqrt{2}d + \frac{(1 + 2\lambda^2)^2}{\sqrt{2}d\lambda^2(1 - 2d\lambda)^2} + \frac{3 + 6\lambda^2}{\sqrt{2}\lambda(2d\lambda - 1)}. \quad (38)$$

As long as $\lambda \gg 1$, the success probability P_{CZ} remains almost constant for a given C . In fact, we need to select appropriate parameters to ensure that the success probability of the entangling gate remains relatively high, while its error is arbitrarily small.

To demonstrate the feasibility of our protocol, we perform numerical simulations of the evolution of the composite system with the full master equation in Eq. (13), instead of the effective master equation in Eq. (14). The initial state of our system is assumed to be

$$|\Psi\rangle_{\text{ini}} = |\Phi\rangle_{\text{ini}} \otimes |\text{vac}\rangle, \quad (39)$$

where $|\Phi\rangle_{\text{ini}}$ represents the initial state of the auxiliary and qubit-encoding atoms, given by

$$|\Phi\rangle_{\text{ini}} = |g\rangle \left[\prod_{k=1}^2 |+\rangle_k \right], \quad (40)$$

where $|+\rangle_k = (|0\rangle_k + |1\rangle_k)/\sqrt{2}$, $|\text{vac}\rangle$ is the vacuum state of the three coupled cavities. We solve the master equation with the QuTiP package [92, 93], and calculate the success probability (P_{CZ}) and fidelity (F_{CZ}) of the gate with the following expressions:

$$P_{CZ} = \sum_{N=0}^2 \text{Tr} [(|g\rangle \langle g| \otimes \mathcal{P}_N \otimes \mathcal{I}) \rho_T(t_{CZ})], \quad (41)$$

$$\rho_{\text{qubit}}(t_{CZ}) = \frac{1}{P_{CZ}} \text{Tr}_{\text{cav}} [\langle g| \rho_T(t_{CZ}) |g\rangle], \quad (42)$$

$$F_{CZ} = \langle \psi | (\mathcal{U} \otimes \mathcal{U}) \rho_{\text{qubit}}(t_{CZ}) (\mathcal{U} \otimes \mathcal{U})^\dagger | \psi \rangle, \quad (43)$$

where Tr and Tr_{cav} are trace operations over the composite system and the cavities, respectively, and \mathcal{I} is the identity operator for the three cavities.

The success probability P_{CZ} and the gate error (infidelity), $1 - F_{CZ}$, are shown in Fig. 2 as a function of the detuning Δ_{E_2}/γ for two different cooperativities $C = 100$ and $C = 600$. In our numerical simulations, we set $\lambda = 10$ to reduce the influence of the off-resonant modes c_2 and c_3 on the gate error. Meanwhile, we assume that $\gamma_g = \gamma_f$, $\kappa = 10\gamma$, $\alpha = \beta = 1$, $\Omega = \Delta_{E_2}/(6C^{1/4})$, and $\Omega_m = 4\gamma C^{1/4}$.

The detunings Δ_{E_1} and Δ_e , given in Eq. (32), are tuned to achieve a total qubit-independent decay rate. The numerical results (marked by symbols) of the success probability P_{CZ} are in agreement with the analytical ones determined by Eq. (37), as shown in Fig. 2(a). The success probability P_{CZ} is almost constant for a given cooperativity C and gradually increases with increasing C . For the aforementioned parameters, $P_{CZ} = 0.56$ can be achieved for $C = 600$.

The fidelity of the heralded nonlocal entangling gate, which is conditioned on the detection of the auxiliary

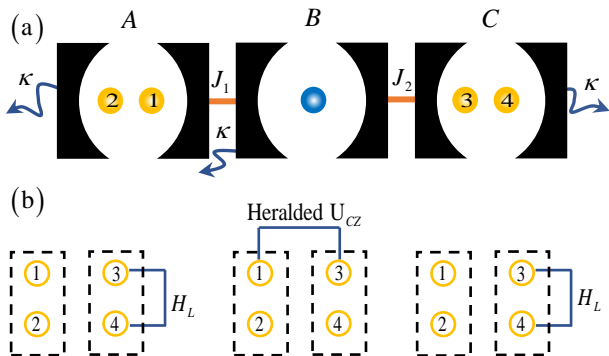


FIG. 3: (a) Schematic diagram of heralded nonlocal entangling gates within a decoherence-free subspace. (b) Implementation scheme of a logical CNOT gate. H_L represents the Hadamard operation on a logical qubit consisting of the atoms 3 and 4, and U_{CZ} represents a CPHASE gate on the atoms 1 and 3 that couple to cavities A and C, respectively.

atom in the state $|g\rangle$, can approach unity in principle. The finite length of the driving field in combination with the finite effective decay from $|E_2\rangle$ to $|g\rangle$ can introduce undetectable errors. Theoretically, the former error leads to a nonadiabatic error of the gate, but which can be suppressed by properly tuning the Rabi frequency Ω of the driving field. At the same time, the latter error can be decreased by increasing the detuning Δ_{E_2} . For a cooperativity $C = 100$, the gate error increases with the detuning Δ_{E_2} , due to the increase in Ω and thus in the nonadiabatic error, and can be less than 2×10^{-3} for $\Delta_{E_2}/\gamma = 100$. For a larger cooperativity $C = 600$, the gate error first decreases and then increases with increasing detuning Δ_{E_2}/γ . A gate error below 3×10^{-4} can be achieved for $C = 600$ and $\Delta_{E_2}/\gamma = 180$, as shown in Fig. 2(b).

V. HERALDED NONLOCAL QUANTUM GATES WITH ENCODING IN A DECOHERENCE-FREE SUBSPACE

In this section, we focus on the implementation of heralded single- and two-qubit gates on logical qubits that are robust against collective random dephasing errors, stemming from the fluctuations of the external fields and, thus, resulting in uncontrolled energy shifts [42]. In the case of the collective dephasing, the symmetry properties of the errors allow to identify a DFS in the Hilbert space of a two-physical-qubit system [47–51], where the two logical basis states can be $|0_L\rangle = |01\rangle$ and $|1_L\rangle = |10\rangle$, and a memory-time enhancement of two orders of magnitude has been experimentally demonstrated for ion-trap systems [50].

Suppose that the qubit-encoding atoms 1 and 2 (3 and 4) are coupled to the cavity A (C) and encode a logical qubit. The cavities A and C interact with the cavity

B through two short fibers or superconducting coaxial cables, as shown in Fig. 3. We assume that there is an auxiliary atom coupled the cavity B. The coupling rate between cavities A (C) and B is J_1 (J_2), and all the three cavities decay with the same rate κ .

In principle, a CPHASE gate, U_L^{CZ} , on these two logical qubits, given by $U_L^{CZ} = \exp(i\pi |1_L 1_L\rangle \langle 1_L 1_L|)$ can be achieved with a heralded nonlocal CPHASE gate $U_{1,3}^{CZ}$ on the atom pair (1, 3) from two logical qubits. The gate $U_{1,3}^{CZ}$ can be implemented with the same method described in the previous sections, while the other two atoms need to be decoupled from the cavities (i.e., by modifying their detunings) during the controlled-phase gate operation. Furthermore, a controlled-NOT (CNOT) gate on two nonlocal logical qubits can be constructed by sandwiching a CPHASE gate with two Hadamard operations on the same logical qubit as follows:

$$\text{CNOT}_L = (I \otimes H_L) \times (U_{13}^{CZ}) \times (I \otimes H_L), \quad (44)$$

where I is the identity on the first logical qubit, U_{13}^{CZ} is a nonlocal CPHASE gate performed on the atom pair (1, 3), and H_L performs the Hadamard transformation on the second logical qubit, as shown in Fig. 3.

The operation of the Hadamard gate on a logical qubit is nontrivial and changes the entanglement between two physical atoms encoding a logical qubit. The logical Hadamard gate can be implemented by a two-qubit entangling gate in combination with single-qubit rotations on two qubit-encoding atoms as follows [59]:

$$H_L = [(HSHZ) \otimes (HSH)] \text{CNOT}_{34} \times [(HSX) \otimes X], \quad (45)$$

where the gate $S = \text{diag}(1, i)$, in the computational basis $\{|0\rangle, |1\rangle\}$, denotes a rotation around the Z -axis by an angle $\pi/2$; H is the standard Hadamard transformation on a single physical qubit; while X and Z are Pauli operators. The CNOT_{34} gate, with the control atom 3 and the target atom 4, can be implemented by

$$\text{CNOT}_{34} = H_4 U_{34}^{CZ} H_4, \quad (46)$$

where H_4 represents the Hadamard transform on the qubit 4, and U_{34}^{CZ} is the heralded CPHASE gate acting on the qubits 3 and 4 that are coupled to the same cavity.

The heralded CPHASE gate U_{34}^{CZ} acting on the qubits 3 and 4 can be achieved in a setup similar to that shown in Fig. 1, except that the cavity A is decoupled from the cavity B, i.e., $J_1 = 0$ and $J_2 = J$, and the heralded nonlocal CPHASE gate is modified to become a compact one, as described in Ref. [71].

In order to explicitly describe the dynamics of the composite system consisting of two cavities and three atoms, we perform a transformation for the two cavity modes and introduce the symmetric and antisymmetric optical modes, $a_{\pm} = (a_B \pm a_C)/\sqrt{2}$. The total Hamiltonian is $H_T = H_e + V + V^\dagger$, where V is the same

as in Eq. (7), while H_e is changed to

$$\begin{aligned}
H_e = & \sum_{k=1}^2 \left\{ \Delta_e |e\rangle_k \langle e| + \frac{g}{\sqrt{2}} [(a_+ - a_-) |e\rangle_k \langle 1| + \text{H.c.}] \right\} \\
& + \Delta_{E_1} |E_1\rangle \langle E_1| + \Delta_{E_2} |E_2\rangle \langle E_2| + 2J a_+^\dagger a_+ \\
& + \frac{gf}{\sqrt{2}} [(a_+ + a_-) |E_1\rangle \langle f| + \text{H.c.}] \\
& + \frac{\Omega_m}{2} (|E_1\rangle \langle E_2| + \text{H.c.}). \tag{47}
\end{aligned}$$

For large detunings ($\Delta_{E_1} \gg \Omega$ and $\Delta_{E_2} \gg \Omega_m$) and a large coupling strength ($J \gg gf$) between the cavities B and C, we can adiabatically eliminate the excited states $|E_1\rangle$ and $|E_2\rangle$ and then obtain a three-photon resonant Raman transition from $|g\rangle$ to $|f\rangle$, by choosing a driving field with frequency

$$\omega_L = \omega_c - \omega_m + \omega_f - \omega_g - J. \tag{48}$$

Such a three-photon resonant Raman transition is resonantly mediated by the antisymmetric mode a_- , while detuned by $2J$ from the symmetric mode a_+ .

Following the procedure in Sec. II, we can implement the heralded near-deterministic CPHASE gate on the qubit-encoding atoms 3 and 4 in the same cavity, which has been discussed in dissipative circuit quantum electrodynamics (QED) systems [71]. We can completely remove the gate errors introduced by the qubit-dependent decay rate by modifying the detunings Δ_e and Δ_{E_1} to be:

$$\frac{\Delta_e}{\gamma} = \frac{1}{2(2D_1 + \bar{G})}, \tag{49}$$

$$\frac{\Delta_{E_1}}{\gamma} = \alpha C (D_1 + \bar{G}), \tag{50}$$

where $D_1 = \sqrt{[\bar{G}^2 + \beta/(\alpha C)]/2}$. In the limit $\{G, C\} \gg 1$, the effective Hamiltonian driving the evolution of the composite system can be described as

$$H_{\text{eff}} = |g\rangle \langle g| \otimes \sum_{n=0}^2 \Delta'_n \mathcal{P}_n, \tag{51}$$

where \mathcal{P}_n is a projector onto the states with n qubit-encoding atoms in the state $|1\rangle$. The corresponding energy shift Δ'_n is given by

$$\Delta'_0 = -\frac{\Gamma D_1}{2}, \tag{52}$$

$$\Delta'_{n>0} = -\frac{\tilde{\Omega}^2}{2\gamma} \frac{n(2D_1 + \bar{G})}{\alpha C (4nD_1^2 + 2nD_1\bar{G} + 1/C)}, \tag{53}$$

where Δ'_0 approaches zero, while $\Delta'_1 \simeq \Delta'_2$ with $|\Delta'_1| \simeq |\Delta'_2| \gg |\Delta'_0|$ for $\{G, C\} \gg 1$. Therefore, we can implement a CPHASE gate on the atoms 3 and 4 by properly tuning the duration of the driving pulse in

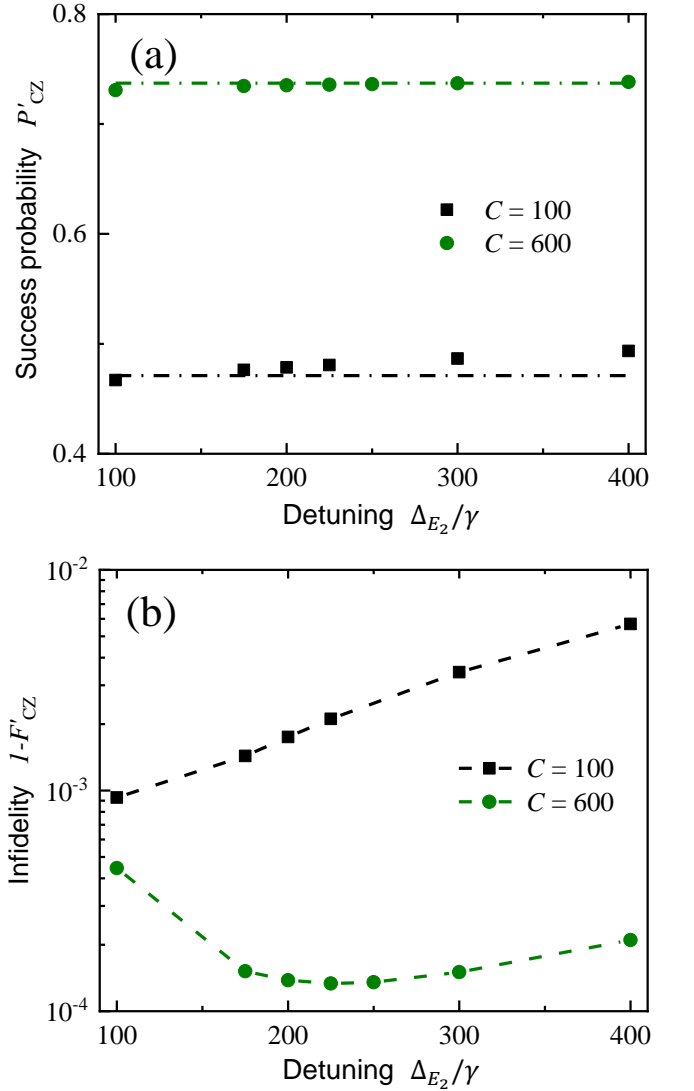


FIG. 4: Numerical simulations for the heralded CPHASE gate on two qubit-encoding atoms, the logical qubit, with two cooperativities: $C = 100$ (black squares) and $C = 600$ (olive solid circles). (a) The success probability P'_{CZ} as a function of the detuning Δ_{E_2}/γ . Simultaneously, we also plot the analytical results (shown by curves), which matches well with the numerical ones. (b) Infidelity $1 - F'_{CZ}$ versus the detuning Δ_{E_2}/γ . All the system parameters and the initial state are the same as those assumed in Fig. 2, except $\lambda = 1.84$.

combination with the single-qubit rotations, according to Eqs. (34) and (35) after replacing Δ_n with Δ'_n .

The success probability P'_{CZ} and the error $(1 - F'_{CZ})$ of the CPHASE gate on two qubit-encoding atoms coupled to the same cavity are of the same formalism as those described in Eqs. (41) and (43), while the density matrix describes the composite system consisting of three atoms and two cavities.

We numerically calculate P'_{CZ} and $(1 - F'_{CZ})$ and demonstrate their dependence on the detuning Δ_{E_2}/γ for different cooperativities ($C = 100$ and $C = 600$),

shown in Fig. 4. All the system parameters and the initial state are the same as those assumed in Fig. 2, except for $\lambda = 1.84$. The success probability P_{CZ} increases with increasing C and can be larger than that of the heralded nonlocal CPHASE gate with $P'_{CZ} = 0.74$ for $C = 600$. Meanwhile, the gate error decreases with C and shows a dependence on detuning Δ_{E_2}/γ , similar to that of the nonlocal CPHASE gate. For $C = 600$, the gate error $1 - F'_{CZ}$ can be suppressed to 1.2×10^{-4} for $\Delta_{E_2}/\gamma = 220$. Therefore, the Hadamard gate in combination with the nonlocal CPHASE gate can be faithfully implemented with the cavity-coupled system in a heralded way.

VI. DISCUSSION AND SUMMARY

Our protocol generalizes the previous proposal of heralded entangling gates [70, 71] on qubits coupled to the same cavity to a nonlocal case by dynamically controlling the evolution rather than by scattering and measuring single photons. The integrated error detection eliminates the limitation of single-photon sources and measurements [87], and enables a high fidelity of the heralded entangling gates at the cost of a smaller success probability. Furthermore, we apply our heralded nonlocal entangling gate to heralded single- and two-qubit quantum gates within a DFS that is immune to collective dephasing noise. The heralded nonlocal entangling gates on qubits belonging to different cavities are suitable for interconnecting individual quantum processors for distributed quantum computing [78] and quantum repeater networks [85, 86].

Our protocol can be experimentally implemented with neutral or artificial atoms coupled to various cavities [4]. As an example, we consider ultracold ^{87}Rb atoms coupled to optical cavities [70]. The relevant energy levels can be encoded as: the two ground states $|g\rangle$ ($|0\rangle$) and $|f\rangle$ ($|1\rangle$) corresponding to the atomic levels $|F = 1, m_f = 1\rangle$ and $|F = 2, m_f = 2\rangle$ of $5^2S_{1/2}$, respectively; and the two excited states $|E_2\rangle$ and $|E_1\rangle$ ($|e\rangle$) corresponding to $|F = 2, m_f = 2\rangle$ and $|F = 3, m_f = 3\rangle$ of

$5^2P_{3/2}$, respectively. Optical cavities with high- Q factors have recently been widely used for quantum information technology [94–96]. The coupling strength g between a cavity and an atom inversely depends on the cavity mode volume, i.e., $g \propto 1/\sqrt{V}$ and can, thus, be significantly enhanced for small mode volume cavities, such as fiber Fabry-Perot cavities [97], photonic crystal cavities [18] and whispering gallery mode cavities [98]. A single-atom cooperativity $C > 500$ for a strong single atom-photon coupling can be achieved for microring resonators [99].

In summary, we have proposed a heralded entangling quantum gate on nonlocal stationary qubits coupled to different cavities. We can faithfully implement a nonlocal entangling gate in a heralded way by dynamically controlling the evolution of a composite system and projecting the auxiliary atom onto a postselected state. We have further showed its application for implementing quantum gates on logical qubits within a DFS. All these distinct characteristics make these quantum gates useful for distributed quantum computation and quantum networks.

ACKNOWLEDGMENTS

This work was supported in part by the National Natural and Science Foundation of China (Grant No. 11904171) and the Fundamental Research Funds for the Central Universities (Grant No. 30922010807). W.Q. was supported in part by the Incentive Research Project of RIKEN. A.M. was supported by the Polish National Science Centre (NCN) under the Maestro Grant No. DEC-2019/34/A/ST2/00081. F.N. is supported in part by: Nippon Telegraph and Telephone Corporation (NTT) Research, the Japan Science and Technology Agency (JST) [via the Quantum Leap Flagship Program (Q-LEAP), and the Moonshot R&D Grant Number JPMJMS2061], the Asian Office of Aerospace Research and Development (AOARD) (via Grant No. FA2386-20-1-4069), and the Foundational Questions Institute Fund (FQXi) via Grant No. FQXi-IAF19-06.

-
- [1] T. D. Ladd, F. Jelezko, R. Laflamme, Y. Nakamura, C. Monroe, and J. L. O’Brien, “Quantum computers,” *Nature (London)* **464**, 45–53 (2010).
 - [2] S. Slussarenko and G. J. Pryde, “Photonic quantum information processing: A concise review,” *Appl. Phys. Rev.* **6**, 041303 (2019).
 - [3] A. F. Kockum and F. Nori, “Quantum bits with josephson junctions,” in *Fundamentals and Frontiers of the Josephson Effect*, edited by F. Tafuri (Springer, New York, 2019) pp. 703–741.
 - [4] I. Buluta, S. Ashhab, and F. Nori, “Natural and artificial atoms for quantum computation,” *Rep. Prog. Phys.* **74**, 104401 (2011).
 - [5] Y. Zhou, E. M. Stoudenmire, and X. Waintal, “What limits the simulation of quantum computers?” *Phys. Rev. X* **10**, 041038 (2020).
 - [6] G.-L. Long, “General quantum interference principle and duality computer,” *Commun. Theor. Phys.* **45**, 825 (2006).
 - [7] I. M. Georgescu, S. Ashhab, and F. Nori, “Quantum simulation,” *Rev. Mod. Phys.* **86**, 153–185 (2014).
 - [8] X. Yuan, “A quantum-computing advantage for chemistry,” *Science* **369**, 1054–1055 (2020).
 - [9] Arute *et al.*, “Quantum supremacy using a programmable superconducting processor,” *Nature (London)* **574**, 505–510 (2019).
 - [10] Y. Wu *et al.*, “Strong quantum computational advantage using a superconducting quantum processor,” *Phys. Rev. Lett.* **127**, 180501 (2021).
 - [11] A. D. King *et al.*, “Scaling advantage over path-integral

- Monte Carlo in quantum simulation of geometrically frustrated magnets,” *Nat. Commun.* **12**, 1113 (2021).
- [12] H.-S. Zhong *et al.*, “Quantum computational advantage using photons,” *Science* **370**, 1460–1463 (2020).
- [13] H.-S. Zhong *et al.*, “Phase-programmable Gaussian boson sampling using stimulated squeezed light,” *Phys. Rev. Lett.* **127**, 180502 (2021).
- [14] L. S. Madsen *et al.*, “Quantum computational advantage with a programmable photonic processor,” *Nature* **606**, 75–81 (2022).
- [15] L.-M. Duan and H. Kimble, “Scalable photonic quantum computation through cavity-assisted interactions,” *Phys. Rev. Lett.* **92**, 127902 (2004).
- [16] K. Koshino, S. Ishizaka, and Y. Nakamura, “Deterministic photon-photon $\sqrt{\text{SWAP}}$ gate using a Λ system,” *Phys. Rev. A* **82**, 010301 (2010).
- [17] A. Reiserer, N. Kalb, G. Rempe, and S. Ritter, “A quantum gate between a flying optical photon and a single trapped atom,” *Nature (London)* **508**, 237–240 (2014).
- [18] T. Tiecke, J. D. Thompson, N. P. de Leon, L. Liu, V. Vuletić, and M. D. Lukin, “Nanophotonic quantum phase switch with a single atom,” *Nature (London)* **508**, 241–244 (2014).
- [19] K. Nemoto, M. Trupke, S. J. Devitt, A. M. Stephens, B. Scharfenberger, K. Buczak, T. Nöbauer, M. S. Everitt, J. Schmiedmayer, and W. J. Munro, “Photonic architecture for scalable quantum information processing in diamond,” *Phys. Rev. X* **4**, 031022 (2014).
- [20] W.-Q. Liu, H.-R. Wei, and L.-C. Kwek, “Low-cost Fredkin gate with auxiliary space,” *Phys. Rev. Appl.* **14**, 054057 (2020).
- [21] C. D. Bruzewicz, J. Chiaverini, R. McConnell, and J. M. Sage, “Trapped-ion quantum computing: Progress and challenges,” *Appl. Phys. Rev.* **6**, 021314 (2019).
- [22] L. Postler *et al.*, “Demonstration of fault-tolerant universal quantum gate operations,” *Nature (London)* **605**, 675–680 (2022).
- [23] W. Qin, A. Miranowicz, G. Long, J. You, and F. Nori, “Proposal to test quantum wave-particle superposition on massive mechanical resonators,” *npj Quantum Inf.* **5**, 58 (2019).
- [24] H.-R. Wei and F.-G. Deng, “Compact quantum gates on electron-spin qubits assisted by diamond nitrogen-vacancy centers inside cavities,” *Phys. Rev. A* **88**, 042323 (2013).
- [25] P.-B. Li, Z.-L. Xiang, P. Rabl, and F. Nori, “Hybrid quantum device with nitrogen-vacancy centers in diamond coupled to carbon nanotubes,” *Phys. Rev. Lett.* **117**, 015502 (2016).
- [26] G. Burkard, V. O. Shkolnikov, and D. D. Awschalom, “Designing a cavity-mediated quantum cphase gate between NV spin qubits in diamond,” *Phys. Rev. B* **95**, 205420 (2017).
- [27] X.-Y. Chen and Z.-Q. Yin, “Universal quantum gates between nitrogen-vacancy centers in a levitated nanodiamond,” *Phys. Rev. A* **99**, 022319 (2019).
- [28] P.-B. Li, Y. Zhou, W.-B. Gao, and F. Nori, “Enhancing spin-phonon and spin-spin interactions using linear resources in a hybrid quantum system,” *Phys. Rev. Lett.* **125**, 153602 (2020).
- [29] C. Y. Hu, A. Young, J. L. O’Brien, W. J. Munro, and J. G. Rarity, “Giant optical faraday rotation induced by a single-electron spin in a quantum dot: Applications to entangling remote spins via a single photon,” *Phys. Rev. B* **78**, 085307 (2008).
- [30] T. Li and F.-G. Deng, “Error-rejecting quantum computing with solid-state spins assisted by low- Q optical microcavities,” *Phys. Rev. A* **94**, 062310 (2016).
- [31] N. Lo Piparo, W. J. Munro, and K. Nemoto, “Quantum multiplexing,” *Phys. Rev. A* **99**, 022337 (2019).
- [32] P. Lodahl, S. Mahmoodian, and S. Stobbe, “Interfacing single photons and single quantum dots with photonic nanostructures,” *Rev. Mod. Phys.* **87**, 347 (2015).
- [33] J.-Q. You and F. Nori, “Atomic physics and quantum optics using superconducting circuits,” *Nature (London)* **474**, 589–597 (2011).
- [34] M. H. Devoret and R. J. Schoelkopf, “Superconducting circuits for quantum information: an outlook,” *Science* **339**, 1169–1174 (2013).
- [35] G. Wendin, “Quantum information processing with superconducting circuits: a review,” *Rep. Prog. Phys.* **80**, 106001 (2017).
- [36] X. Gu, A. F. Kockum, A. Miranowicz, Y.-x. Liu, and F. Nori, “Microwave photonics with superconducting quantum circuits,” *Phys. Rep.* **718**, 1–102 (2017).
- [37] L. Viola, E. Knill, and S. Lloyd, “Dynamical decoupling of open quantum systems,” *Phys. Rev. Lett.* **82**, 2417–2421 (1999).
- [38] B. Pokharel, N. Anand, B. Fortman, and D. A. Lidar, “Demonstration of fidelity improvement using dynamical decoupling with superconducting qubits,” *Phys. Rev. Lett.* **121**, 220502 (2018).
- [39] P. Zanardi and M. Rasetti, “Holonomic quantum computation,” *Phys. Lett. A* **264**, 94–99 (1999).
- [40] G. F. Xu, J. Zhang, D. M. Tong, E. Sjöqvist, and L. C. Kwek, “Nonadiabatic holonomic quantum computation in decoherence-free subspaces,” *Phys. Rev. Lett.* **109**, 170501 (2012).
- [41] P. Z. Zhao, K. Z. Li, G. F. Xu, and D. M. Tong, “General approach for constructing Hamiltonians for nonadiabatic holonomic quantum computation,” *Phys. Rev. A* **101**, 062306 (2020).
- [42] D. A. Lidar, I. L. Chuang, and K. B. Whaley, “Decoherence-free subspaces for quantum computation,” *Phys. Rev. Lett.* **81**, 2594–2597 (1998).
- [43] A. F. Kockum, G. Johansson, and F. Nori, “Decoherence-free interaction between giant atoms in waveguide quantum electrodynamics,” *Phys. Rev. Lett.* **120**, 140404 (2018).
- [44] N. Shammah, S. Ahmed, N. Lambert, S. De Liberato, and F. Nori, “Open quantum systems with local and collective incoherent processes: Efficient numerical simulations using permutational invariance,” *Phys. Rev. A* **98**, 063815 (2018).
- [45] J. Zhang, Z.-Y. Zhou, L.-A. Wu, and J. You, “Protection of logical qubits via optimal state transfers,” *Phys. Rev. Appl.* **11**, 044023 (2019).
- [46] B. M. Terhal, “Quantum error correction for quantum memories,” *Rev. Mod. Phys.* **87**, 307–346 (2015).
- [47] L.-A. Wu, P. Zanardi, and D. A. Lidar, “Holonomic quantum computation in decoherence-free subspaces,” *Phys. Rev. Lett.* **95**, 130501 (2005).
- [48] J. Q. You, X. Hu, and F. Nori, “Correlation-induced suppression of decoherence in capacitively coupled cooper-pair boxes,” *Phys. Rev. B* **72**, 144529 (2005).
- [49] M. Mićuda, R. Stárek, J. Fiurášek, and R. Filip,

- “Decoherence-resilient linear optical two-qubit quantum gate,” *Phys. Rev. Appl.* **14**, 054066 (2020).
- [50] T. Monz *et al.*, “Realization of universal ion-trap quantum computation with decoherence-free qubits,” *Phys. Rev. Lett.* **103**, 200503 (2009).
- [51] Y.-F. Qiao, J.-Q. Chen, X.-L. Dong, B.-L. Wang, X.-L. Hei, C.-P. Shen, Y. Zhou, and P.-B. Li, “Generation of Greenberger-Horne-Zeilinger states for silicon-vacancy centers using a decoherence-free subspace,” *Phys. Rev. A* **105**, 032415 (2022).
- [52] P. Xue and Y.-F. Xiao, “Universal quantum computation in decoherence-free subspace with neutral atoms,” *Phys. Rev. Lett.* **97**, 140501 (2006).
- [53] L.-X. Cen, Z. D. Wang, and S. J. Wang, “Scalable quantum computation in decoherence-free subspaces with trapped ions,” *Phys. Rev. A* **74**, 032321 (2006).
- [54] E. Brion, L. H. Pedersen, K. Molmer, S. Chutia, and M. Saffman, “Universal quantum computation in a neutral-atom decoherence-free subspace,” *Phys. Rev. A* **75**, 032328 (2007).
- [55] Z. J. Deng, M. Feng, and K. L. Gao, “Preparation of entangled states of four remote atomic qubits in decoherence-free subspace,” *Phys. Rev. A* **75**, 024302 (2007).
- [56] Q. Chen and M. Feng, “Quantum-information processing in decoherence-free subspace with low-Q cavities,” *Phys. Rev. A* **82**, 052329 (2010).
- [57] X.-K. Song, H. Zhang, Q. Ai, J. Qiu, and F.-G. Deng, “Shortcuts to adiabatic holonomic quantum computation in decoherence-free subspace with transitionless quantum driving algorithm,” *New J. Phys.* **18**, 023001 (2016).
- [58] S. L. Wu, X. L. Huang, H. Li, and X. X. Yi, “Adiabatic evolution of decoherence-free subspaces and its shortcuts,” *Phys. Rev. A* **96**, 042104 (2017).
- [59] M. Zwerger, B. P. Lanyon, T. E. Northup, C. A. Muschik, W. Dür, and N. Sangouard, “Quantum repeaters based on trapped ions with decoherence-free subspace encoding,” *Quantum Sci. Technol.* **2**, 044001 (2017).
- [60] J. Zhang, S. J. Devitt, J. Q. You, and F. Nori, “Holonomic surface codes for fault-tolerant quantum computation,” *Phys. Rev. A* **97**, 022335 (2018).
- [61] D. Farfurnik, R. M. Pettit, Z. Luo, and E. Waks, “Single-shot readout of a solid-state spin in a decoherence-free subspace,” *Phys. Rev. Appl.* **15**, L031002 (2021).
- [62] X. Hu, F. Zhang, Y. Li, and G. Long, “Optimizing quantum gates within decoherence-free subspaces,” *Phys. Rev. A* **104**, 062612 (2021).
- [63] L.-N. Sun, F.-Q. Guo, Z. Shan, M. Feng, L.-L. Yan, and S.-L. Su, “One-step implementation of Rydberg nonadiabatic noncyclic geometric quantum computation in decoherence-free subspaces,” *Phys. Rev. A* **105**, 062602 (2022).
- [64] T. Chen, P. Shen, and Z.-Y. Xue, “Robust and fast holonomic quantum gates with encoding on superconducting circuits,” *Phys. Rev. Appl.* **14**, 034038 (2020).
- [65] Y.-H. Chen, R. Stassi, W. Qin, A. Miranowicz, and F. Nori, “Fault-tolerant multiqubit geometric entangling gates using photonic cat-state qubits,” *Phys. Rev. Appl.* **18**, 024076 (2022).
- [66] G.-R. Feng, G.-F. Xu, and G.-L. Long, “Experimental realization of nonadiabatic holonomic quantum computation,” *Phys. Rev. Lett.* **110**, 190501 (2013).
- [67] Z. Zhu, T. Chen, X. Yang, J. Bian, Z.-Y. Xue, and X. Peng, “Single-loop and composite-loop realization of nonadiabatic holonomic quantum gates in a decoherence-free subspace,” *Phys. Rev. Appl.* **12**, 024024 (2019).
- [68] Y. Xu, Z. Hua, T. Chen, X. Pan, X. Li, J. Han, W. Cai, Y. Ma, H. Wang, Y. P. Song, Z.-Y. Xue, and L. Sun, “Experimental implementation of universal nonadiabatic geometric quantum gates in a superconducting circuit,” *Phys. Rev. Lett.* **124**, 230503 (2020).
- [69] J. Z. Blumoff *et al.*, “Fast and high-fidelity state preparation and measurement in triple-quantum-dot spin qubits,” *PRX Quantum* **3**, 010352 (2022).
- [70] J. Borregaard, P. Kómár, E. M. Kessler, A. S. Sørensen, and M. D. Lukin, “Heralded quantum gates with integrated error detection in optical cavities,” *Phys. Rev. Lett.* **114**, 110502 (2015).
- [71] W. Qin, X. Wang, A. Miranowicz, Z. Zhong, and F. Nori, “Heralded quantum controlled-phase gates with dissipative dynamics in macroscopically distant resonators,” *Phys. Rev. A* **96**, 012315 (2017).
- [72] Y.-H. Kang, Z.-C. Shi, J. Song, and Y. Xia, “Heralded atomic nonadiabatic holonomic quantum computation with Rydberg blockade,” *Phys. Rev. A* **102**, 022617 (2020).
- [73] J. Borregaard, P. Kómár, E. M. Kessler, M. D. Lukin, and A. S. Sørensen, “Long-distance entanglement distribution using individual atoms in optical cavities,” *Phys. Rev. A* **92**, 012307 (2015).
- [74] J. Borregaard, A. S. Sørensen, J. I. Cirac, and M. D. Lukin, “Efficient quantum computation in a network with probabilistic gates and logical encoding,” *Phys. Rev. A* **95**, 042312 (2017).
- [75] W. Qin, A. Miranowicz, P.-B. Li, X.-Y. Lü, J. Q. You, and F. Nori, “Exponentially enhanced light-matter interaction, cooperativities, and steady-state entanglement using parametric amplification,” *Phys. Rev. Lett.* **120**, 093601 (2018).
- [76] J. I. Cirac, A. K. Ekert, S. F. Huelga, and C. Macchiavello, “Distributed quantum computation over noisy channels,” *Phys. Rev. A* **59**, 4249–4254 (1999).
- [77] Y. L. Lim, A. Beige, and L. C. Kwek, “Repeat-until-success linear optics distributed quantum computing,” *Phys. Rev. Lett.* **95**, 030505 (2005).
- [78] L. Jiang, J. M. Taylor, A. S. Sørensen, and M. D. Lukin, “Distributed quantum computation based on small quantum registers,” *Phys. Rev. A* **76**, 062323 (2007).
- [79] S.-B. Zheng, C.-P. Yang, and F. Nori, “Arbitrary control of coherent dynamics for distant qubits in a quantum network,” *Phys. Rev. A* **82**, 042327 (2010).
- [80] H.-J. Briegel, W. Dür, J. I. Cirac, and P. Zoller, “Quantum repeaters: The role of imperfect local operations in quantum communication,” *Phys. Rev. Lett.* **81**, 5932–5935 (1998).
- [81] L. Jiang, J. M. Taylor, K. Nemoto, W. J. Munro, R. Van Meter, and M. D. Lukin, “Quantum repeater with encoding,” *Phys. Rev. A* **79**, 032325 (2009).
- [82] T.-J. Wang, S.-Y. Song, and G. L. Long, “Quantum repeater based on spatial entanglement of photons and quantum-dot spins in optical microcavities,” *Phys. Rev. A* **85**, 062311 (2012).
- [83] W. J. Munro, A. M. Stephens, S. J. Devitt, K. A. Harrison, and K. Nemoto, “Quantum communication without the necessity of quantum memories,” *Nat. Photonics* **6**, 777–781 (2012).

- [84] Y.-B. Sheng, L. Zhou, and G.-L. Long, “Hybrid entanglement purification for quantum repeaters,” *Phys. Rev. A* **88**, 022302 (2013).
- [85] S. Wehner, D. Elkouss, and R. Hanson, “Quantum internet: A vision for the road ahead,” *Science* **362**, eaam9288 (2018).
- [86] P.-S. Yan, L. Zhou, W. Zhong, and Y.-B. Sheng, “A survey on advances of quantum repeater,” *EPL* **136**, 14001 (2021).
- [87] A. Reiserer and G. Rempe, “Cavity-based quantum networks with single atoms and optical photons,” *Rev. Mod. Phys.* **87**, 1379 (2015).
- [88] J. Cho, D. G. Angelakis, and S. Bose, “Heralded generation of entanglement with coupled cavities,” *Phys. Rev. A* **78**, 022323 (2008).
- [89] A. Serafini, S. Mancini, and S. Bose, “Distributed quantum computation via optical fibers,” *Phys. Rev. Lett.* **96**, 010503 (2006).
- [90] M. J. Kastoryano, F. Reiter, and A. S. Sørensen, “Dissipative preparation of entanglement in optical cavities,” *Phys. Rev. Lett.* **106**, 090502 (2011).
- [91] F. Reiter and A. S. Sørensen, “Effective operator formalism for open quantum systems,” *Phys. Rev. A* **85**, 032111 (2012).
- [92] J. R. Johansson, P. D. Nation, and F. Nori, “Qutip: An open-source python framework for the dynamics of open quantum systems,” *Comput. Phys. Commun.* **183**, 1760–1772 (2012).
- [93] J. Johansson, P. Nation, and F. Nori, “Qutip 2: A python framework for the dynamics of open quantum systems,” *Comput. Phys. Commun.* **184**, 1234–1240 (2013).
- [94] B. Hacker, S. Welte, G. Rempe, and S. Ritter, “A photon–photon quantum gate based on a single atom in an optical resonator,” *Nature (London)* **536**, 193–196 (2016).
- [95] H. Takahashi, E. Kassa, C. Christoforou, and M. Keller, “Strong coupling of a single ion to an optical cavity,” *Phys. Rev. Lett.* **124**, 013602 (2020).
- [96] H. J. Kimble, “The quantum internet,” *Nature (London)* **453**, 1023–1030 (2008).
- [97] M. Brekenfeld, D. Niemietz, J. D. Christesen, and G. Rempe, “A quantum network node with crossed optical fibre cavities,” *Nat. Phys.* **16**, 647–651 (2020).
- [98] S. Yang, Y. Wang, and H. Sun, “Advances and prospects for whispering gallery mode microcavities,” *Adv. Opt. Mater.* **3**, 1136–1162 (2015).
- [99] T.-H. Chang, B. M. Fields, M. E. Kim, and C.-L. Hung, “Microring resonators on a suspended membrane circuit for atom-light interactions,” *Optica* **6**, 1203–1210 (2019).